Journal of Materials Chemistry A

ARTICLE

Shape-controlled octahedral cobalt disulfide nanoparticles supported on nitrogen and sulfur-doped graphene/carbon nanotube composites for oxygen reduction in acidic electrolyte

D.C. Higgins, F. Hassan, M. H. Seo, J. Y. Choi, M. A. Hoque, D. U. Lee, Z. Chen*

Replacement of expensive platinum-based catalysts at the cathode of fuel cells by low-cost alternatives represents an important milestone to achieve significant system cost reductions. In this work, single crystal cobalt disulfide (CoS_2) octahedral nanoparticles supported on graphene/carbon nanotube composites were prepared as oxygen reduction reaction (ORR) catalysts in acidic electrolyte. During the simplistic, one-pot solvothermal synthesis, the nanostructured carbon supports were also simultaneously doped with nitrogen and sulfur. Time dependent studies elucidated the growth process of the {111} facet encased octahedra that could only be prepared when carbon support materials were incorporated into the reaction mixture. Through computational simulations, the shape directed growth process was found to be driven thermodynamically towards surface energy minimization. Control experiments and spectroscopy characterization were also used to investigate the occurrence and nature of nitrogen and sulfur doping into the graphitic structure of the graphene/carbon nanotube composite support. The impact of carbon support on ORR activity was clear, with the graphene/carbon nanotube composite supported CoS_2 octahedra (CoS_2-CG) outperforming CoS_2 supported on just graphene or carbon nanotubes. Additionally, CoS_2-CG provided an on-set potential (0.78 V vs. RHE) and half-wave potential (0.66 V vs. RHE) that was 60 mV and 150 mV higher than the CoS_2 particle agglomerates formed when no carbon support was included during catalyst preparation. This improved activity can be attributed to the beneficial properties of the nitrogen and sulfur doped graphene/carbon nanotube composite support, and also may arise due to the more favourable oxygen adsorption on the (111) surface of the octahedral particles predicted by theoretical calculations. By combining the synergistic properties of the graphene/carbon nanotube composite and unique shape controlled single crystal CoS_2 nanoparticles, CoS_2-CG is presented as an emerging catalyst for the ORR in fuel cells.

Introduction

Nanostructured metal chalcogenides have emerged on the forefront of materials science and technology research as promising functional materials for application in a variety of energy technologies.[1] Cobalt sulfide, exhibiting interesting phase-dependent electronic, magnetic and catalytic properties,[2,3] boasts great potential for application in energy conversion and storage technologies, including fuel cells,[4-9] supercapacitors,[10-12] lithium ion batteries[13-15] and photoelectrochemical dye-sensitized solar cells.[16-18] The controllable synthesis of highly

crystalline and mono-phase nanostructures of cobalt sulfide is however very challenging, yet desirable from an application standpoint. This is owing to the highly oxophilic nature of cobalt and the complicated stoichiometry of cobalt sulfide that consists of various phases, all with different physicochemical properties.[3] Using cobalt sulfide nanoparticles in conjunction with high surface area nanostructured carbon supports, such as graphene or carbon nanotubes (CNTs), can also be highly advantageous. These supports in particular provide interconnecting mesostructured scaffolds that can facilitate good nanoparticle dispersion and electron transport. The structural, surface and electron properties of graphene or CNTs

can furthermore be modulated through doping with various heteroatoms, such as nitrogen or sulfur.[19-23] In addition to inducing unique functionality, these dopant species can also provide beneficial carbon support-nanoparticle interactions.[20, 24-26]

One notable field of application for cobalt sulfide is as a non-precious oxygen reduction reaction (ORR) catalyst for polymer electrolyte fuel cells (PEFCs). As a replacement to the expensive platinum catalysts required to facilitate the ORR,[27] this would alleviate some of the uncertainty surrounding the long-term commercial success of PEFCs, owing to the volatile material costs and monopolized global distribution of this precious metal. This technological challenge has inspired significant non-precious ORR catalyst research efforts in recent years, with several promising replacements including, transition metal chalcogenides and oxides, or high temperature heat treated transition metal-nitrogen-carbon complexes (dubbed "M-N-C", where M is generally Co, or Fe) demonstrated.[28, 29] The M-N-C systems remain the most extensively investigated class of non-precious metal catalyst to date, with significant improvements to ORR activity and operational durability realized in recent years.[30-33] Despite this, the multi-step fabrication process, including high temperature (i.e. > 800 °C) heat treatment(s) results in heterogeneous, multi-component structures. This leads to extensive debate over the identity and nature of the ORR active site structures present in these catalysts, even after over two decades of research activities, rendering the rational design of improved performance M-N-C catalysts a very challenging endeavour. It is therefore of interest to develop and investigate alternative non-precious ORR catalyst technologies, prepared by simplistic, energy efficient and scalable techniques that can provide highly homogeneous active phase structures. This will provide opportunity for researchers and scientists to understand and improve the ORR kinetic processes occurring on these well-defined nanostructured surfaces, in an attempt to ultimately eliminate the dependence on Pt-based catalysts.

In this work, we report the unique solvothermal preparation of shape controlled, single crystal cobalt disulfide (CoS_2) octahedron particles supported on nitrogen and sulfur doped CNT/graphene composites (CoS_2-CG). This single step, relatively low temperature (220 °C) approach offers several notable advantages, including an inexpensive, low-energy consuming and one-pot scalable synthesis, along with excellent CoS_2 shape control and facet exposure achieved without the addition of any template or surfactant species. With excellent phase purity, the prepared CoS_2-CG nanostructures are demonstrated to provide the highest performance towards the ORR in acidic electrolyte (0.1 M $HClO_4$) reported to date for non-precious metal chalcogenide materials. Through careful investigation, we elucidate the CoS_2 octahedron formation process and propose a growth mechanism. Additionally, we clearly demonstrate the performance advantages of using CNT/graphene composites as supports for the octahedron nanoparticles, and investigate the nature of nitrogen and sulfur doping into the graphitic lattice of the nanostructured carbon materials. Nitrogen and sulfur co-doped graphene materials are generally prepared by high temperature heat treatment approaches, and this work highlights successful double-doping by a solvothermal process, providing practical implications for various applications such as ORR catalysis in alkaline conditions.[21, 23, 34]

Results and discussion

Material preparation and characterization

Three primary materials were developed in this work by a single-step solvothermal approach using different nanostructured carbon supports, including CoS_2 supported on graphene (CoS_2-G), CNTs (CoS_2-C) and a CNT/graphene composite (CoS_2-CG). Transmission electron microscopy (TEM) images of each of these materials are provided in **Figures 1a**, **1b** and **1c**, respectively. Consistent with results from scanning electron microscopy (SEM) imaging that show the overall homogeneous morphology (**Figure S1**), it was observed that regardless of the nanostructured carbon support type, shape controlled octahedral CoS_2 particles were grown on the carbon surface, with no unsupported particles formed in solution. For CoS_2-CG (**Figure 1c**, **Figure S1c**), octahedral nanoparticles were clearly intermixed with CNTs that had assembled on the sheet-like surface of graphene. This CNT assembly likely arises from the amphiphilic surfactant-like nature of graphene oxide (GO), consisting of hydrophilic oxygen-containing surface species that render it highly dispersible in aqueous solutions, along with basal plane aromatic regions[35]. When dispersed in solution with CNTs, the aromatic groups present in each component can provide a strong attachment through π-π interactions,[36, 37] resulting in the observed assembly of CNTs on the surface of graphene sheets, and no free CNTs observed on the TEM grid. A high resolution TEM image of a shape controlled nanoparticle from the CoS_2-CG sample is provided in **Figure 1d**, consisting of a single crystal with an octahedral morphology. The lattice space measurement of 0.318 nm is in close agreement with the theoretical {111} spacing of CoS_2 (0.319 nm), indicating that the crystalline octahedral particle is encased by the {111} facets. This observation is consistent with the results of Bao *et al.*,[38] who demonstrated the biomolecule-assisted hydrothermal preparation of free-standing microscale Co_3S_4 octahedrons enclosed by the {111} surfaces.

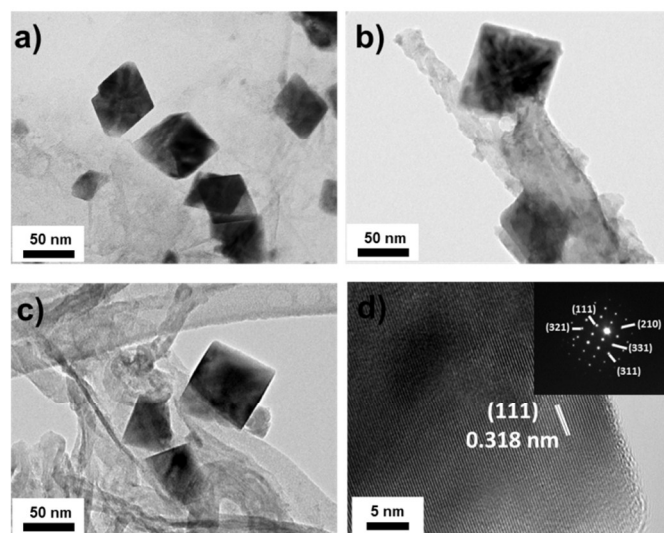**Figure 1.** TEM images of (a) CoS_2-G, (b) CoS_2-C and (c) CoS_2-CG. (d) High resolution TEM image of a single crystal CoS_2 octahedron particle along with (inset) SAED pattern.

Interestingly, when only CNTs were used as the nanostructured carbon support, the distribution of CoS_2 particles on CoS_2-C was reduced, with larger average crystallite sizes observed. This indicates that the high concentration of

surface functional species on the GO starting materials provides a beneficial impact in terms of providing nucleation and anchoring sites for well distributed nanoparticles.[24] The impact of support selection was also indicated by the results of carrying out the solvothermal process in the absence of any nanostructured carbon support. Only large particle agglomerate structures were obtained (**Figure S1d**), with no evidence of octahedron nanostructure formation.

Operating in scanning transmission electron microscopy (STEM) mode, energy dispersive x-ray (EDX) atomic mapping was carried out on a bundle of octahedral particles of varying size in order to determine the atomic content and distributions of the CoS_2-CG materials. With colour mapping images provided in **Figure 2a**, the octahedron particles consist of concentrated regions of both cobalt and sulfur, with some sulfur species observed throughout the CNT/graphene supports, indicative of sulfur doping into the graphitic structures during solvothermal processing. The atomic composition of a single octahedral particle was investigated by carrying out EDX analysis, with the obtained spectra (**Figure S2**) indicating a Co:S ratio of 36.3 to 63.4 at. %, in close agreement with the expected atomic content of the CoS_2 phase.
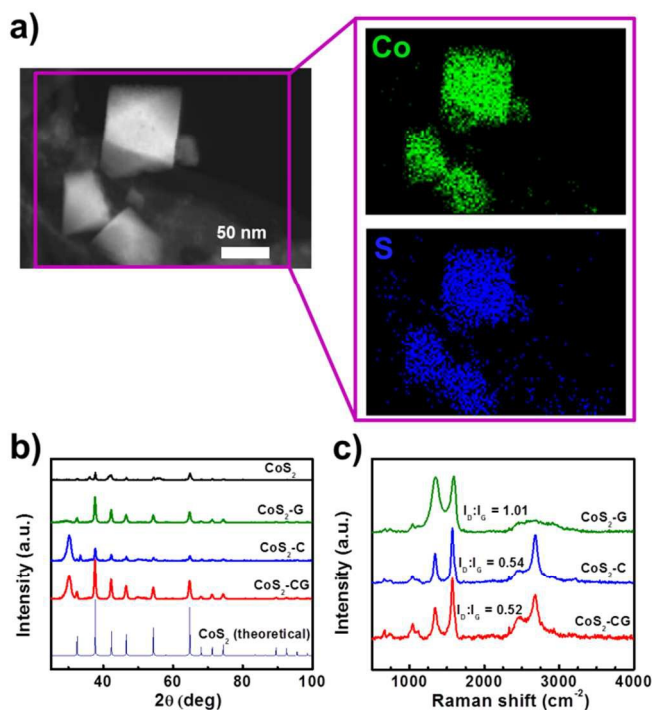

Figure 2. (a) EDX colour mapping of CoS2-CG, (b) XRD patterns of prepared samples and theoretical CoS2 pattern, and (c) Raman spectra for CoS2-G, CoS2-C and CoS2-CG.

X-ray diffraction (XRD) was used to confirm the phase structure of the prepared materials, with diffraction patterns of the prepared samples provided in **Figure 2b**. The diffraction peaks observed for CoS_2-G, CoS_2-C and CoS_2-CG were in direct agreement with the standard pattern of cubic CoS_2 with a lattice parameter of 0.554 nm (86351-ICSD). When prepared in the absence of any nanostructured carbon support, the diffraction pattern of the as-prepared CoS_2 materials demonstrated the CoS_2 phase, however minor CoS diffraction peaks were also observed. This reiterates the important role of the nanostructured carbon supports in preparing well-dispersed,

homogeneous CoS_2 nanoparticles. The CoS phase could potentially be present as an intermediate species for CoS_2 formation that became entrapped within the large agglomerates during particle growth, or could arise due to the effect (or lack thereof) that the nanostructured carbon species with electrostatically charged surface functional species has on the synthesis process.

Provided in **Figure 2C** are the Raman spectra for CoS_2-G, CoS_2-C and CoS_2-CG. Each sample clearly shows a "D-band" peak located at ca. 1339 cm^{-2}, attributed to defect induced structural vibrations and a "G-band" peak located at ca. 1580 cm^{-2} and attributed to the E_{2g} vibration spectra of sp^2 bonded carbon. These peaks, in addition to the 2D-band peak demonstrated at ca. 2683 cm^{-2} are characteristic of graphitic materials and arise from the nanostructured carbon materials used to support CoS_2 particles. Commonly the D-band to G-band peak ration (I_D:I_G) is used to gauge the degree of structural disorder present in CNT or graphene based materials.[39] CoS_2-G demonstrates an I_D:I_G ratio of 1.01, which is in agreement with the values obtained previously for graphene-based materials[40, 41] and indicating that the solvothermal process was successful in reducing the surface oxygen species of GO. The I_D:I_G ratios of CoS_2-C and CoS_2-CG were similar at 0.54 and 0.52, respectively. This value is consistent with results reported for CNT-based materials reported recently[41] and also provides indication that the CNT component of the composite supported CoS_2-CG contributes primarily to the observed Raman spectra, most likely due to the fact that CNTs are observed to be assembled on the surface of the graphene sheets.

Using CoS_2-CG as a representative sample, the Co2p and S2p spectra obtained by x-ray photoelectron spectroscopy (XPS) are provided in **Figure 3a** and **3b**, respectively. The Co2p spectra displays three spin-orbit couples, with the lower binding energy peaks displayed in the figure and located at ca. 778.9, 781.0 and 782.95 eV, respectively. The first peak comprises the majority of Co atoms scanned and can be attributed to the Co^{2+} species of CoS_2, an observation consistent with results of previous spectroscopic investigations on cobalt sulfide materials.[3, 5, 38] The two minor peaks located at higher binding energies could be due to the presence of Co-NH bonds formed between residual ammonia species from the decomposition of thiourea[38] or satellite shake up peaks.[42] More rigorous investigations are required to elucidate the exact source of these observed peaks, although they comprise only a small amount of the surface cobalt ions scanned and therefore are not of significant concern. The S2p peak in **Figure 3b** demonstrates a main peak comprised or two $Sp_{1/2}$ and $Sp_{3/2}$ doublets. The first doublet, with peaks located at 162.4 and 163.6 eV are attributed to the CoS_2 phase.[5, 42] The second pair, with peaks located at 164.5 and 165.6 eV are attributed to thiophenic sulfur species incorporated into the CNT/graphene support matrix.[43, 44] While these results, in accordance with the previously discussed EDX colour mapping indicate successful doping of the nanostructured carbon supports through the solvothermal process, this phenomenon, including nitrogen doping, will be investigated and discussed in more detail later on. There is an additional pair of peaks in the S2p spectra observed at ca. 169.0 eV, which can be attributed to oxidized sulfur species, potentially sulfates,[45] that are present in small quantities on the surface of the developed materials.
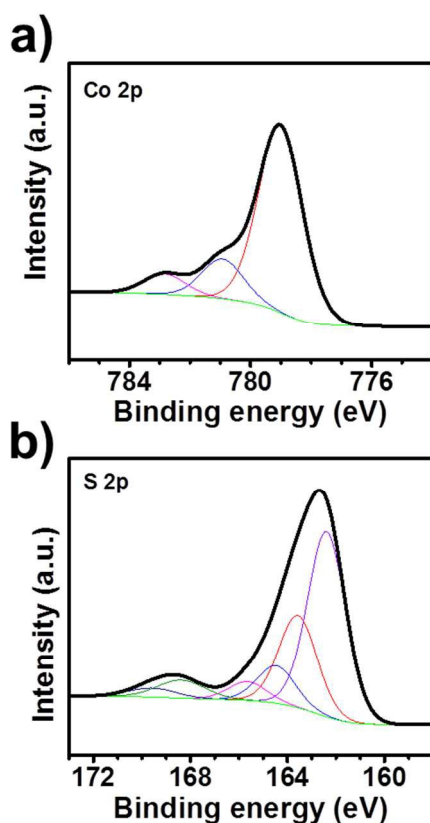
Figure 3. High resolution XPS (a) Co2p and (b) S2p spectra of CoS₂-CG.

CoS₂ octahedron growth process

To understand the mechanistic process of CoS₂ octahedron particle formation and growth, a time dependent synthesis investigation was carried out using graphene as the representative support material. After initially heating the solvothermal reaction temperature up to 120 °C and maintaining it for 10 hours, the temperature was further increased to 220 °C, after which the reaction was interrupted at various time intervals by removing the solvothermal reactor from the oven. After 0.5 h (**Figure 4a**, **Figure S3a**), only small, irregularly shaped nanoparticles were observed on the surface of the graphene sheets. This structure is consistent with the materials that resulted when a reaction temperature of only 120 °C was used for the entire solvothermal reaction (CoSG-120), and the nanoparticles were determined to be amorphous based on XRD, high resolution TEM imaging and select area electron diffraction (SAED) patterns provided in **Figure S4**. As the reaction time at 220 °C is lengthened to 2.5 h, the formation of larger, crystalline nanoparticles is observed (**Figure 4b**, **Figure S3b**). Further increasing the reaction time to 5 h, disappearance of the majority of amorphous nanoparticles occurs, and there is an abundance of larger particle structures starting to exhibit the single crystal octahedron morphology (**Figure 4c**, **Figure S3c**). Finally after a reaction time of 10 h, only octahedron nanoparticles, comprised of single crystals with varying sizes well-distributed across the surface of graphene remain (**Figure 4d**, **Figure S3d**), with minimal changes to morphology observed with a further increase in the reaction time to 20 h. Drawing on these observations, a schematic outlining the crystal phase transformations and growth occurring on the

surface of graphene during the solvothermal reaction is provided in **Figure 5**. It can also be seen that at increasing reaction times, the structure of the graphene substrates gradually evolve. Initially this material shows a relatively smooth, sheet-like structure (**Figure 4a, S3a**). Throughout the reaction process and associated to the reduction of GO, the substrate takes on a wrinkled configuration with increasing amounts of edge plane exposure (**Figures 4b-d, S3b-d**).
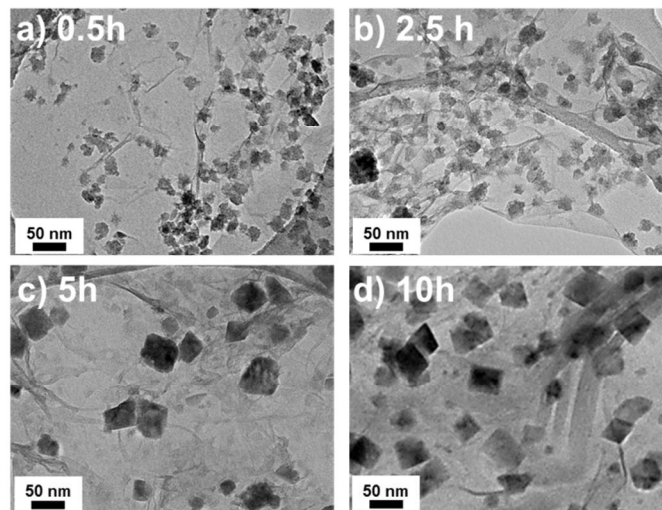

Figure 4. TEM images of the time dependent growth of CoS₂ supported on graphene held at 220 °C for (a) 0.5 h, (b) 2.5 h, (c) 5 h and (d) 10 h.

Figure 5. Proposed growth schematic of CoS₂ octahedron nanoparticles supported on nitrogen and sulfur doped graphene.

Reduction and doping of graphene with nitrogen and sulfur

With the formation and growth process of octahedral CoS₂ nanoparticles elucidated, of particular importance in the present work is also the reduction and simultaneous doping (i.e., nitrogen and sulfur) processes occurring in the nanostructured carbon supports. Because the presence of CoS₂ nanoparticles on the surface of the nanostructured carbon supports will confound the results of these spectroscopic investigations, graphene, CNT and CNT/graphene composite samples were prepared under the same reaction conditions, albeit in the absence of a cobalt precursor. These samples were found to be doped with both nitrogen and sulfur, and are therefore referred to as NS-G, NS-C and NS-CG, respectively. The absence of cobalt precursor had a negligible impact on the microstructure of the obtained materials, with SEM images of NS-G, NS-C and NS-CG

provided in **Figure S5a**, **S5b** and **S5c**, respectively. These materials demonstrated a very similar structure to those prepared with cobalt precursor, although as expected, without CoS_2 octahedron nanoparticles decorated on the surface. XPS was used to confirm the successful reduction of GO during the solvothermal process, with the oxygen surface content of NS-G quantified to be 7.21 at. %, significantly lower than the ca. 35 at. % commonly reported for GO[40].

High resolution S2p and N1s spectra for the nitrogen/sulfur-doped nanostructured carbon supports are provided in **Figure S6**. The obtained signals indicate that the solvothermal procedure used in the present work were capable of incorporating both sulfur and nitrogen heteroatom dopants into the CNT/graphene materials. Double doping of nanostructured carbons with more than one element has been reported before, commonly accomplished by high temperature heat treatment processes in the presence of heteroatom containing precursors.[41, 46] Reports on double doping by hydrothermal or solvothermal processes however are very rare,[47, 48] and to the best of our knowledge, only one report exists for the double doping of graphene or CNT structures with nitrogen and sulfur by hydro/solvothermal procedures.[49] NS-G was found to have the highest concentration of sulfur and nitrogen dopants within the structure, with a surface concentration of 2.98 and 2.75 at. %, respectively. This likely arises due to the highly tunable surface structures of GO, containing an abundance of oxygen-containing functional species that can serve as reactive sites for heteroatom incorporation[35]. For NS-C, the sulfur and nitrogen contents were lower at 0.71 and 0.95 at. %, respectively, indicating the incorporation of heteroatom species into functionalized CNTs by "post-treatment" methods is relatively more difficult, an observation consistent with previous investigations[41, 50]. The sulfur and nitrogen contents of NS-CG (0.68 and 1.09 at. %, respectively) were similar to that of NS-C, suggesting that the majority of XPS signal arises from the CNT constituent assembled on the surface of graphene sheets in the composite arrangement.

The S2p spectra of all three materials (**Figure S6a-c**) could be deconvoluted into the $S2p_{1/2}$ and $S2p_{3/2}$ doublet peaks of thiophenic sulfur, located at 164.1 and 165.3 eV, respectively.[43, 51] Thiophenic sulfur species reside on the edge plane of graphene/CNT in a 5-membered heterocyclic ring arrangement. The N1s spectra of each sample was deconvoluted intro three individual contributions arising from pyridinic (ca. 398.6 eV), pyrrolic (400.1 eV) and graphitic (401.2 eV) nitrogen species [39, 52]. NS-G (**Figure S6d**) was comprised of mainly pyrrolic nitrogen species, however both pyridinic and graphitic nitrogen was observed in sufficient quantities. On the other hand, almost all of the nitrogen atoms scanned in NS-C (**Figure S6e**) were of pyrollic form, residing on edge plane of the CNTs and bonded to carbon in a 5-membered ring arrangement. It appears that the incorporation of pyridinic or graphitic nitrogen species into the 6-membered ring structures of CNTs is difficult at the relatively low (220 °C) temperature used during the solvothermal synthesis. At higher temperatures (i.e. > 800 °C) it has been well established that the pyridinic species are not as stable, at which conditions increased relative graphitic nitrogen contents are commonly observed.[53, 54] The N1s spectra of NS-CG (**Figure S6f**) indicates that pyrrolic nitrogen species are still dominant in the composite arrangement, although small peaks arising from graphitic and pyridinic nitrogen species are observed, most likely arising from the underlying doped graphene sheet structures.

Proposed growth mechanism

The complex reaction mixture consisting of multiple organic and inorganic species, in combination with the "black box" nature of solvothermal syntheses renders *in situ* monitoring and speciation to elucidate the exact mechanistic process of material preparation very difficult. Notwithstanding these challenges, based on fundamental information available in the literature and results of our *ex situ* experimental results, we propose a mechanism for the fabrication of nitrogen and sulfur-doped graphene supported CoS_2 octahedrons. After reacting solvothermally for 10h at 120 °C, amorphous particles were observed decorated on the surface of GO sheets (**Figure S4**). This most likely consists of Co-based intermediates (i.e. oxides, carbonates or hydroxides) formed through the decomposition of cobalt acetate,[55] and nucleated on the oxygen containing functional sites of GO owing to the favourable interactions of these species with inorganic nanoparticles.[24]

When the solvothermal reaction temperature is increased to 220 °C, this exceeds the decomposition temperature of thiourea (ca. 187 °C), a process that generates primarily ammonia, carbon disulfide and thiocyanic acid as the byproducts.[56] Owing to the isomeric complexity of thiourea with numerous potential decomposition intermediates and reaction pathways,[57] it is also likely that under the solvothermal reaction conditions the formation of other sulfur-containing species can occur. One such species is hydrogen sulfide, which has interestingly been attributed as a sulfur source for cobalt sulfide formation,[58] however is not a commonly observed species during the thermal decomposition of thiourea.[56, 59] Regardless, when the reaction temperature is increased to 220 °C, the decomposition of thiourea is evidenced by transformation of the solution colour to yellow, which becomes more pronounced at increasing reaction times (**Figure S7**). After 30 min at 220 °C, only slight discolouration of the solvothermal solution is observed (**Figure S7b**) and amorphous Co-based nanoparticles comprise the majority of species in existence on the surface of the graphene sheets (**Figure 4a**). This provides indication that the entire reaction mixture has not reached a uniform temperature of 220 °C, and/or the decomposition of thiourea and the CoS_2 formation reactions did not have enough time to proceed.

Once the thiourea species have a sufficient reaction temperature and time to decompose, the high concentration of available sulfur-containing intermediates will attach the amorphous nanoparticles decorating the graphene surface. This results in the formation or irregularly shaped CoS_2 particles that are observed after holding the reaction temperature at 220 °C for 2.5 h (**Figure 4b**). At increased reaction times, more CoS_2 species continue to form and Ostwald ripening processes comprise the subsequent structural transformations observed. During this time period, inhomogeneous CoS_2 species migrate and rearrange to form single crystal octahedral structures encased by the {111} crystal facets. This morphology likely forms as it the most thermodynamically stable structure due to the relatively low surface energy of the (111) surface in comparison to other CoS_2 surface structures as predicted by theoretical simulations (*vide infra*).

In terms of the graphene based supports, it is not only expected that the covalently bonded oxygen functional species in GO play a crucial role in Co-based nanoparticle nucleation and growth,[24] but also serve as anchoring sites for the incorporation of heteroatom dopant species.[35] As a primary product of thiourea decomposition, ammonia (NH_3) species will be formed within the solvothermal reaction vessel. NH_3 is

commonly used as a precursor for the simultaneous nitrogen doping and reduction of GO materials by annealing treatments,[40, 41, 53, 54] and more recently by hydro/solvothermal methods.[60, 61] Additionally, EG is a well-known reducing agent for GO during solvothermal synthesis,[62] and in tandem with NH_3 results in the effective reduction and nitrogen doping of the graphene supports. On the other hand, identification of the exact sulfur containing intermediate(s) formed during thiourea decomposition that are responsible for sulfur doping of graphene requires further, more stringent fundamental investigations.

Electrochemical performance evaluation

ORR polarization plots for all of the prepared samples in 0.1 M $HClO_4$ and at an electrode rotation speed of 1600 rpm are provided in **Figure 6a**, with onset potential and half-wave potential ($E_{1/2}$) values summarized in **Table 1** versus the reversible hydrogen electrode (RHE). Linear potential sweeps at electrode rotation speeds varying from 100 to 2500 rpm are provided for CoS_2-CG in **Figure 6b**, and for CoS_2-G (**Figure S8**), CoS_2-C (**Figure S9**) and as-prepared CoS_2 (**Figure S10**) in the supporting information. All of the nanostructured carbon supported CoS_2 octahedron catalysts displayed similar ORR onset potentials, suggesting that the active site structures present in these catalysts are the same. The unsupported, as-prepared CoS_2 materials demonstrated an on-set potential that was ca. 40-60 mV lower, along with reduced ORR current densities throughout almost the entire potential range investigated. The reduced performance of as-prepared CoS_2 can likely be linked to the large agglomerate structure of the catalyst, with ORR activity resembling that reported previously for a CoS_2 thin film structure.[5] The increased onset potential of the carbon supported CoS_2 octahedrons could also arise due to the more favourable adosprtion energy of oxygen on the (111) surface of CoS_2 in comparison to the (001) and (110) surfaces, as determined from our theoretical simulations *vide infra*. The supported octahedrons consist of only {111} surface facets, which could therefore be advantageous for ORR kinetics in comparison to the unsupported CoS_2 agglomerates consisting of a mix of various surface structures. Additionally, the minor presence of the CoS phase as illustrated by XRD within the unsupported CoS_2 could provide an impact on ORR performance, albeit to an unknown extent.

Table 1. Electrochemical performance evaluation results.

Parameter (V *vs.* RHE)	CoS_2-CG	CoS_2-G	CoS_2-C	CoS_2
Onset potential[a]	0.78	0.76	0.76	0.72
$E_{1/2}$	0.66	0.64	0.61	0.51

[a]Taken as the potential that the current density reaches 0.1 $mAcm^{-2}$.

It is clear that the incorporation of nanostructured carbon supports into the solvothermal reaction mixture can facilitate the formation of single crystal, shape controlled octahedral CoS_2 nanoparticles immobilized within a conductive network that can provide significant ORR performance enhancements. Of the three materials investigated, CoS_2-CG provides the best ORR performance, with a polarization curve resemblant of high ORR activity catalysts, demonstrating a current density that levels off at lower electrode potentials owing to the onset of mass transport limitations. Comparing the performance of

CoS_2-G and CoS_2-C can provide some understanding regarding the impact of nanostructured carbon support type on ORR activity. Interestingly, CoS_2-G demonstrates slightly higher current densities at high electrode potentials (> 0.63 V *vs.* RHE). In this region, ORR kinetics play a dominant role in the observed catalyst performance, which can likely be attributed to the increased dispersion of well-defined CoS_2 octahedral crystals with smaller average sizes on CoS_2-G. This in turn provides a larger number of ORR active sites in order to facilitate the electrochemical reduction. Additionally, the increased nitrogen and sulfur dopant concentrations in the nanostructured carbon support for CoS_2-G could provide favourable catalyst-support interactions that beneficially influence ORR kinetics, similar to the effect commonly observed in Pt/doped-carbon catalyst systems.[43, 63, 64] At potentials below ca. 0.63 V *vs.* RHE, CoS_2-C provides relatively higher current densities that CoS_2-G. This can most likely be attributed to the highly porous, interconnected catalyst layer structures formed by one-dimensional CNTs. This provides ample pathways for electronic conductivity and access for O_2 reactant molecules, contributing to the increased current densities observed in the potential region that transport (electronic/reactant) properties play a dominant role.
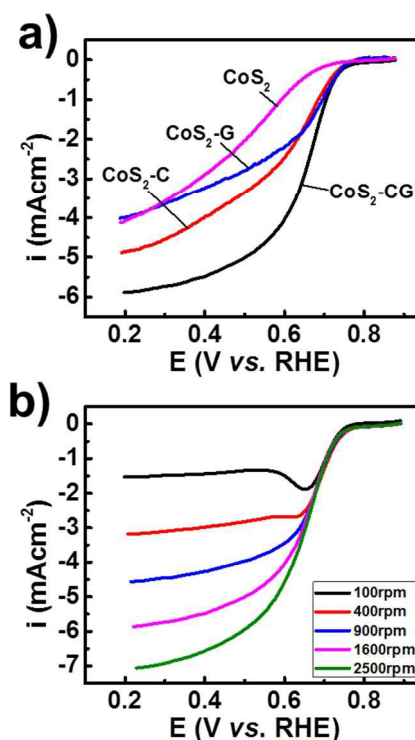

Figure 6. ORR polarization curves (a) at 1600 rpm for all samples, and (b) at various electrode rotation rates for CoS_2-CG.

The half-wave potential for CoS_2-CG is 0.66 V *vs.* RHE, a ca. 20 and 50 mV improvement over that of CoS_2-G and CoS_2-C, respectively. Additionally, Koutecky-Levich analysis[30, 39] indicated excellent selectivity towards the overall four electron ORR mechanism, with the number of electrons calculated to be greater than 3.7 over the entire range of potentials investigated. All of these results indicate that the microstructure of CoS_2-CG provides an ideal balance of inherent ORR active site structure density and turnover frequency, along with reactant access. This likely arises due to the complementary contributions of

each component, whereby the graphene provides excellent octahedral nanoparticle dispersion owing to the high surface areas and ease of functionalization, and CNTs provide highly interconnected, conductive and porous morphologies that can facilitate the rapid access of electrons and oxygen throughout the entire catalyst layer. This notion is supported by the results of Brunauer–Emmett–Teller (BET) analysis, indicating a surface area of 123.9 $m^2 g^{-1}$ for CoS_2-CG, which is higher than CoS_2-C (96.1 $m^2 g^{-1}$) yet lower than CoS_2-G (150.0 $m^2 g^{-1}$). The advantages of this synergistic arrangement have also been previously demonstrated for ORR activity in alkaline electroytes[60, 65, 66], solar cell,[67] lithium-ion battery[68] and supercapacitor[69-71] applications. Drawing on this, CoS_2-CG demonstrates a half-wave potential that is comparable to several precious metal (i.e. Ru) based chalcogenide materials reported previously.[72] Further comparison can be made to the most active non-precious metal chacogenide reported previously,[4] consisting of $Co_{1-x}S$ particles supported on reduced GO ($Co_{1-x}S$/RGO) and prepared by a two-step synthesis method employing a heat treatment process. CoS_2-CG demonstrates a comparable onset potential, although provides a current density of 1.3 $mAcm^{-2}$ at an electrode potential of 0.7 V vs. RHE, an over 15% improvement in comparison to $Co_{1-x}S$/RGO (1.1 $mAcm^{-2}$). Combined with a simplistic preparation process, shape controlled CoS_2 octahedron nanoparticles supported on nitrogen and sulfur doped CNT/graphene composites comprises the best performance non-precious metal chalcogenide ORR catalyst reported to date.

Computational simulation results

Figure S11 shows the fully relaxed bulk CoS_2 structure. After stabilization, the lattice parameters of CoS_2 were evaluated to be 5.505, 5.505 and 5.505 Å, consistent with previous experimental work[73] and theoretical diffraction pattern data. From the bulk structure of CoS_2, slab models for the (111), (001) and (110) surfaces were designed as shown in **Figure 7a**, **b** and **c**, respectively. During model relaxation, we allowed the upper layers to relax, while maintaining the bottom five layers fixed in their bulk positions. The surface energy per unit area (σ) was calculated by equation (1):

$$\sigma = \frac{1}{A}[E_{slab} - nE_{bulk}] \qquad (1)$$

Here, E_{slab} is the total energy of a slab with CoS_2 layers and E_{bulk} is the reference total energy per unit area of the bulk system. For the (111), (001) and (110) surfaces, the surface energies were evaluated to be 0.836, 1.497 and 1.328 J m^{-2}, respectively. It is clearly seen that the order of thermodynamic stability for the relaxed surfaces of CoS_2 are in the order of (111) > (110) > (001). Therefore, the CoS_2 octahedron morphology, encapsulated by (111) surfaces as confirmed by SAED and high resolution TEM imaging, is very likely a result of surface energy minimization occurring through the solvothermal synthesis.

We then wanted to investigate the chemical adsorption energies of atomic oxygen on the various CoS_2 surface structures. It is well known that the binding strength of adsorbates play an important role governing ORR activity. This is due to the Sabatier principle that states that catalytic reaction rates are favourable when there exists an appropriately moderate interaction between the adsorbate species and the catalytically active surface.[74-76] **Figures 7d**, **e** and **f** illustrate the oxygen adsorption sites on the (111), (001) and (110) surface structures of CoS_2, respectively. The adsorption energy ($E_{ads,O}$) was then calculated according to equation (2):

$$\Delta E_{ads,O} = E_{O-CoS2} - E_O - E_{CoS_2} \qquad (2)$$

Here, E_{O-CoS2}, E_O and E_{CoS2} are energies of the CoS_2 surface with adsorbed oxygen, the isolated oxygen atom and a clean CoS_2 surface, respectively. The adsorption energies of oxygen (ΔE_{ads}) were evaluated to be -3.940, -3.928 and -5.297 eV for the (111), (001) and (110) surfaces of CoS_2, respectively. Taking into account the E_{ads} value of -4.36 eV for oxygen on a bulk Pt(111) surface (calculated for a 1/4 monolayer of oxygen on a (2 × 2) unit cell, and consistent with values previously reported in the literature[77, 78]), significantly weaker oxygen adsorption in observed on the (111) and (001) surfaces of CoS_2, whereas significantly stronger oxygen adsorption is observed on the (111) surface. Regardless, the (111) surface of CoS_2 has an oxygen adsorption energy that is closest to the optimal value of ca. -4.08 eV, that can be achieved on Pt_3Ni surfaces.[78] This highlights that the (111) surface of CoS_2 can provide the highest activity towards the ORR among others investigated, and can serve to explain the relatively excellent performance of the {111} facet encased octahedrons observed through RDE evaluation.
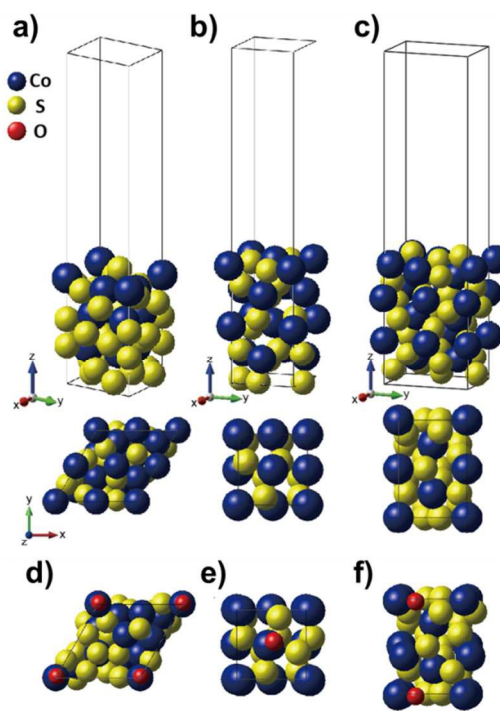

Figure 7. Slab models of CoS_2 with the (a) (111), (b) (001) and (c) (110) surfaces. Oxygen adsorbed on the (d) (111), (e) (001) and (f) (110) surfaces.

Conclusions

Using a one-pot solvothermal technique, we prepared CoS_2 octahedra nanoparticles supported on nitrogen and sulfur doped graphene, CNTs or a graphene/CNT composite. The incorporation of these nanostructured carbon supports into the reaction mixture was essential for achieving excellent CoS_2 phase purity and well-defined octahedra nanoparticles encased by the {111} facets. The growth of the CoS_2 nanoparticles was investigated by a time-dependent study, and was found to occur first by amorphous nanoparticle formation, followed by the continuous evolution into single crystal octahedral achieved after 10 hours of reaction time at 220 °C. This evolution is very

likely thermodynamically driven, owing to our computational simulations revealing that the (111) surface of CoS_2 possesses a significantly lower surface energy than (001) and (110). The simultaneous reduction and doping of the GO and HNO_3-CNT precursors was probed by conducting control experiments in the absence of the cobalt precursors. After the solvothermal reaction, the nanostructured carbon supports were doped with nitrogen and sulfur hetero-atoms, primarily in the pyrollic and thiophenic forms, respectively. Electrochemical half-cell testing in 0.1 M $HClO_4$ revealed that CoS_2-CG provided an ORR on-set and half-wave potential of 0.78 and 0.66 V *vs.* RHE, respectively. The performance was higher than that of CoS2-C and CoS_2-G, highlighting the synergistic benefits of using the graphene/CNT composite arrangements as a support material. Significantly improved ORR activity of CoS_2-CG was also observed in comparison to the CoS_2 nanoparticle agglomerate structured formed when no nanostructured carbon supports were included in the reaction mixture. These performance likely arise due to the theoretical calculations that indicate a more favourable adsorption energy of oxygen on the (111) surface of CoS_2 that the octahedral are composes of. By coupling the synergistic effects of the graphene/CNT composite support with the well-dispersed {111} facet terminated single crystal octahedral nanoparticles, CoS_2-CG is presented as the most active transition metal-chalcogenide towards the ORR reported to date.

Experimental methods

CoS_2-CG synthesis

GO was used as the starting material and was prepared by a modified Hummer's method as reported previously.[79] Commercial CNTs were functionalized by refluxing in 6M HNO_3 for 6h (HNO_3-CNT)[80] to improve the dispersion in ethylene glycol (EG) solvent and interactions with ionic precursor species. In a typical synthesis, 15 mg of GO and 15 mg of HNO_3-CNTs were well-dispersed in 11 mL of EG by ultrasonication for 4 h. Meanwhile, two separate aqueous solutions containing 150 mg/mL of thiourea and 10 mg/mL of cobalt acetate tetrahydrate were prepared and mixed thoroughly by magnetic stirring. Using a pipette, 2 mL of each aqueous precursor solution was then added to the GO/HNO_3-CNT/EG solution, and the total volume of the mixture was increased to 20 mL by the addition of EG. This solution was then ultrasonicated for an additional 30 min to ensure adequate precursor mixing, and was then transferred to a 25 mL Teflon-lined autoclave and tightly sealed. The solvothermal synthesis was carried out by heating the mixture to 120 °C and holding it for 10 h, and then further increasing the temperature to 220 °C, where it remained for an additional 10 h. After cooling, the product was separated by centrifugation, washed thoroughly with DDI water and acetone, and collected by lyophilization. CoS_2 octahedrons supported on just CNTs (CoS_2-C) or graphene (CoS_2-G) were prepared by the same procedure, however using 30 mg of HNO_3-CNT or 30 mg of GO as the nanostructured carbon precursor, respectively. Pure CoS_2 was also prepared in the absence of any nanostructured carbon supports.

Physicochemical characterization

SEM images were obtained using a LEO FESEM 1530. TEM was carried out on a JEOL 2010F equipped with EDX analysis for elemental quantification and atomic dispersion mapping

obtained in STEM mode. XRD patterns were obtained for all samples with cobalt radiation (wavelength = 1.789 Angstroms). Raman spectra was carried out on a Bruker Senterra Raman Microscope operating with a wavelength of 532 nm. XPS was carried out using a monochromatic Al K_α X-ray source (Thermal Scientific). The BET surface areas were determined by N_2 adsorption at 77 K (Micromeritics ASAP 2020). Prior to the BET analysis, catalyst samples were degassed by helium for at least 2 h at 473 K to remove any impurities.

Electrochemical evaluation

All electrochemical testing was carried out in a conventional three-electrode glass cell in 0.1 M $HClO_4$. A RHE and graphite rod were used as the reference and counter electrodes, respectively. The working electrode, consisting of a 0.19635 cm^2 glassy carbon disc encased in a Teflon sheath was cleaned and polished with alumina paste prior to each use. Catalyst ink was prepared by ultrasonically dispersing 4 mg of catalyst in 1 mL of isopropanol containing 0.05 wt. % Nafion ionomer. 30 uL of catalyst ink was then micro-pipetted onto the surface of the glassy carbon working electrode by sequential 10 uL depositions, leading to an overall electrode loading of ca. 0.6 $mgcm^{-2}$. ORR activity was measured under oxygen saturated electrolyte conditions by sweeping the electrode potential from 1.05 to 0.05 V *vs.* RHE, at a scan rate of 10 mVs^{-1}. Capacitive contributions were eliminated by subtracting background currents obtained under the same testing conditions, although under nitrogen saturated electrolyte. All ORR polarization curves were collected for uncompensated electrolyte resistance.[81]

Computational simulations

The total energies of CoS_2 were calculated using the Vienna *ab initio* simulation package (VASP) program[82] with the implemented DFT method.[83, 84] The electron exchange-correlation energy was described by the Perdew, Burke and Ernzerhof (PBE) functional,[85] which employs the spin-polarized generalized gradient approximation (GGA).[86,87] The core electrons were replaced by projector augmented wave (PAW) pseudo-potentials.[88, 89] The valence electrons were described by Kohn-Sham wave functions, which were expanded with a plane-wave basis set. A cutoff energy of 520 eV was used. All ions were fully relaxed during the structural optimization until the total energy was converged within 10^{-4} eV. A gamma point mesh with $(15 \times 15 \times 15)$ k points was used for the CoS_2 (1×1) unit cell to sample the Brillouin zone for bulk calculation. Periodic boundary conditions were imposed on the CoS_2 unit cell in terms of each surface direction of (111), (110) and (001), and a vacuum space of 20 Å was employed to avoid interactions between top and bottom surface. To calculate the total energies of CoS_2 on different surface directions, we only used a gamma point mesh of $(5 \times 5 \times 1)$, and utilized the Methfessel-Paxton smearing method.[90]

Acknowledgements

Notes and references

Department of Chemical Engineering, Waterloo Institute for Nanotechnology, Waterloo Institute of Sustainable Energy, University of Waterloo, 200 University Ave. W, Waterloo, ON, N2L 3G1, Canada. *E-mail: zhwchen@uwaterloo.ca

1. M.R. Gao, Y.F. Xu, J. Jiang, S.H. Yu, *Chemical Society Reviews,* 2013, **42**, 2986.

2. N. Kumar, N. Raman, A. Sundaresan, *Zeitschrift für anorganische und allgemeine Chemie,* 2014, **640**, 1069.

3. Q. Liu, J. Zhang, *CrystEngComm,* 2013, **15**, 5087.

4. H. Wang, Y. Liang, Y. Li, H. Dai, *Angewandte Chemie International Edition,* 2011, **50**, 10969.

5. L. Zhu, D. Susac, M. Teo, K.C. Wong, P.C. Wong, R.R. Parsons, D. Bizzotto, K.A.R. Mitchell, S.A. Campbell, *Journal of Catalysis,* 2008, **258**, 235.

6. Y.X. Zhou, H.B. Yao, Y. Wang, H.L. Liu, M.R. Gao, P.K. Shen, S.H. Yu, *Chemistry – A European Journal,* 2010, **16**, 12000.

7. J.S. Jirkovský, A. Björling, E. Ahlberg, *The Journal of Physical Chemistry C,* 2012, **116**, 24436.

8. G. Wu, N.H. Mack, W. Gao, S. Ma, R. Zhong, J. Han, J.K. Baldwin, P. Zelenay, *ACS Nano,* 2012, **6**, 9764.

9. C. Zhao, D. Li, Y. Feng, *Journal of Materials Chemistry A,* 2013, **1**, 5741.

10. Q. Wang, L. Jiao, H. Du, Y. Si, Y. Wang, H. Yuan, *Journal of Materials Chemistry,* 2012, **22**, 21387.

11. J. Xiao, L. Wan, S. Yang, F. Xiao, S. Wang, *Nano Letters,* 2014, **14**, 831.

12. A.N. Grace, R. Ramachandran, M. Vinoba, S.Y. Choi, D.H. Chu, Y. Yoon, S.C. Nam, S.K. Jeong, *Electroanalysis,* 2014, **26**, 199.

13. J. Wang, S.H. Ng, G.X. Wang, J. Chen, L. Zhao, Y. Chen, H.K. Liu, *Journal of Power Sources,* 2006, **159**, 287.

14. Q. Wang, L. Jiao, Y. Han, H. Du, W. Peng, Q. Huan, D. Song, Y. Si, Y. Wang, H. Yuan, *The Journal of Physical Chemistry C,* 2011, **115**, 8300.

15. Y. Gu, Y. Xu, Y. Wang, *ACS Applied Materials & Interfaces,* 2013, **5**, 801.

16. J.Y. Lin, J.H. Liao, S.W. Chou, *Electrochimica Acta,* 2011, **56**, 8818.

17. C.W. Kung, H.W. Chen, C.Y. Lin, K.C. Huang, R. Vittal, K.C. Ho, *ACS Nano,* 2012, **6**, 7016.

18. E. Bi, H. Chen, X. Yang, W. Peng, M. Gratzel, L. Han, *Energy & Environmental Science,* 2014, **7**, 2637.

19. D. Geng, Y. Chen, Y. Chen, Y. Li, R. Li, X. Sun, S. Ye, S. Knights, *Energy & Environmental Science,* 2011, **4**, 760.

20. Y. Chen, J. Wang, H. Liu, M.N. Banis, R. Li, X. Sun, T.-K. Sham, S. Ye, S. Knights, *The Journal of Physical Chemistry C,* 2011, **115**, 3769.

21. J.P. Paraknowitsch, A. Thomas, *Energy & Environmental Science,* 2013, **6**, 2839.

22. H. Wang, T. Maiyalagan, X. Wang, *ACS Catalysis,* 2012, **2**, 781.

23. H. Wang, M. Xie, L. Thia, A. Fisher, X. Wang, *The Journal of Physical Chemistry Letters,* 2013, **5**, 119.

24. Y. Liang, Y. Li, H. Wang, H. Dai, *Journal of the American Chemical Society,* 2013, **135**, 2013.

25. B. Xia, Y. Yan, X. Wang, X.W. Lou, *Materials Horizons,* 2014, **1**, 379.

26. M.N. Banis, S. Sun, X. Meng, Y. Zhang, Z. Wang, R. Li, M. Cai, T.-K. Sham, X. Sun, *The Journal of Physical Chemistry C,* 2013, **117**, 15457.

27. J.W.D. Ng, M. Tang, T.F. Jaramillo, *Energy & Environmental Science,* 2014, **7**, 2017.

28. Z. Chen, D. Higgins, A. Yu, L. Zhang, J. Zhang, *Energy & Environmental Science,* 2011, **4**, 3167.

29. F. Jaouen, E. Proietti, M. Lefevre, R. Chenitz, J.-P. Dodelet, G. Wu, H.T. Chung, C.M. Johnston, P. Zelenay, *Energy & Environmental Science,* 2011, **4**, 114.

30. P. Zamani, D. Higgins, F. Hassan, G. Jiang, J. Wu, S. Aburedent, Z. Chen, *Electrochimica Acta,* 2014, **139**, 111.

31. G. Wu, K.L. More, C.M. Johnston, P. Zelenay, *Science,* 2011, **332**, 443.

32. H.T. Chung, C.M. Johnston, K. Artyushkova, M. Ferrandon, D.J. Myers, P. Zelenay, *Electrochemistry Communications,* 2010, **12**, 1792.

33. E. Proietti, F. Jaouen, M. Lefèvre, N. Larouche, J. Tian, J. Herranz, J.-P. Dodelet, *Nature Communications,* 2011, **2**, 416.

34. J. Xu, G. Dong, C. Jin, M. Huang, L. Guan, *ChemSusChem,* 2013, **6**, 493.

35. V. Chabot, D. Higgins, A. Yu, X. Xiao, Z. Chen, J. Zhang, *Energy & Environmental Science,* 2014, **7**, 1564.

36. C. Zhang, L. Ren, X. Wang, T. Liu, *The Journal of Physical Chemistry C,* 2010, **114**, 11435.

37. L. Qiu, X. Yang, X. Gou, W. Yang, Z.-F. Ma, G.G. Wallace, D. Li, *Chemistry – A European Journal,* 2010, **16**, 10653.

38. S.J. Bao, Y. Li, C.M. Li, Q. Bao, Q. Lu, J. Guo, *Crystal Growth & Design,* 2008, **8**, 3745.

39. D. Higgins, Z. Chen, Z. Chen, *Electrochimica Acta,* 2011, **56**, 1570.

40. D. Higgins, Z. Chen, D.U. Lee, Z. Chen, *Journal of Materials Chemistry A,* 2013, **1**, 2639.

41. D.C. Higgins, M.A. Hoque, F. Hassan, J.-Y. Choi, B. Kim, Z. Chen, *ACS Catalysis,* 2014, **4**, 2734.

42. H. van der Heide, R. Hemmel, C.F. van Bruggen, C. Haas, *Journal of Solid State Chemistry,* 1980, **33**, 17.

43. D. Higgins, M.A. Hoque, M.H. Seo, R. Wang, F. Hassan, J.-Y. Choi, M. Pritzker, A. Yu, J. Zhang, Z. Chen, *Advanced Functional Materials,* 2014, **24**, 4325.

44. Z. Yang, Z. Yao, G. Li, G. Fang, H. Nie, Z. Liu, X. Zhou, X.a. Chen, S. Huang, *ACS Nano,* 2011, **6**, 205.

45. Z.P. Xu, R. Xu, H.C. Zeng, *Nano Letters,* 2001, **1**, 703.

46. J. Liang, Y. Jiao, M. Jaroniec, S.Z. Qiao, *Angewandte Chemie International Edition,* 2012, **51**, 11496.

47. S.M. Jung, E.K. Lee, M. Choi, D. Shin, I.Y. Jeon, J.M. Seo, H.Y. Jeong, N. Park, J.H. Oh, J.B. Baek, *Angewandte Chemie International Edition,* 2014, **53**, 2398.

48. S.A. Wohlgemuth, R.J. White, M.G. Willinger, M.M. Titirici, M. Antonietti, *Green Chemistry,* 2012, **14**, 1515.

49. Y. Su, Y. Zhang, X. Zhuang, S. Li, D. Wu, F. Zhang, X. Feng, *Carbon,* 2013, **62**, 296.

50. Q. Shi, F. Peng, S. Liao, H. Wang, H. Yu, Z. Liu, B. Zhang, D. Su, *Journal of Materials Chemistry A,* 2013, **1**, 14853.

51. Y. Chang, F. Hong, C. He, Q. Zhang, J. Liu, *Advanced Materials,* 2013, **25**, 4794.

52. D.C. Higgins, J. Wu, W. Li, Z. Chen, *Electrochimica Acta,* 2012, **59**, 8.

53. D.U. Lee, H.W. Park, D. Higgins, L. Nazar, Z. Chen, *Journal of The Electrochemical Society,* 2013, **160**, F910.

54. X. Li, H. Wang, J.T. Robinson, H. Sanchez, G. Diankov, H. Dai, *Journal of the American Chemical Society,* 2009, **131**, 15939.

55. T. Wanjun, C. Donghua, *Chem. Pap.,* 2007, **61**, 329.

56. S. Wang, Q. Gao, J. Wang, *The Journal of Physical Chemistry B,* 2005, **109**, 17281.

57. Z.D. Wang, M. Yoshida, B. George, *Computational and Theoretical Chemistry,* 2013, **1017**, 91.

58. W. Dong, X. Wang, B. Li, L. Wang, B. Chen, C. Li, X. Li, T. Zhang, Z. Shi, *Dalton Transactions,* 2011, **40**, 243.

59. J. Madarász, G. Pokol, *J Therm Anal Calorim,* 2007, **88**, 329.

60. P. Chen, T.Y. Xiao, Y.H. Qian, S.S. Li, S.H. Yu, *Advanced Materials,* 2013, **25**, 3192.

61. P. Chen, J.J. Yang, S.S. Li, Z. Wang, T.Y. Xiao, Y.H. Qian, S.H. Yu, *Nano Energy,* 2013, **2**, 249.

62. C. Nethravathi, M. Rajamathi, *Carbon,* 2008, **46**, 1994.

63. D.C. Higgins, D. Meza, Z. Chen, *The Journal of Physical Chemistry C,* 2010, **114**, 21982.

64. Y. Chen, J. Wang, H. Liu, M.N. Banis, R. Li, X. Sun, T.K. Sham, S. Ye, S. Knights, *The Journal of Physical Chemistry C,* 2011, **115**, 3769.

65. S. Ratso, I. Kruusenberg, M. Vikkisk, U. Joost, E. Shulga, I. Kink, T. Kallio, K. Tammeveski, *Carbon,* 2014, **73**, 361.

66. H.W. Park, D.U. Lee, Y. Liu, J. Wu, L.F. Nazar, Z. Chen, *Journal of The Electrochemical Society,* 2013, **160**, A2244.

67. V.C. Tung, L.M. Chen, M.J. Allen, J.K. Wassei, K. Nelson, R.B. Kaner, Y. Yang, *Nano Letters,* 2009, **9**, 1949.

68. Y. Hu, X. Li, J. Wang, R. Li, X. Sun, *Journal of Power Sources,* 2013, **237**, 41.

69. D. Yu, L. Dai, *The Journal of Physical Chemistry Letters,* 2009, **1**, 467.

70. Q. Cheng, J. Tang, J. Ma, H. Zhang, N. Shinya, L.C. Qin, *Physical Chemistry Chemical Physics,* 2011, **13**, 17615.

71. H. Sun, X. You, J. Deng, X. Chen, Z. Yang, J. Ren, H. Peng, *Advanced Materials,* 2014, **26**, 2868.

72. Y. Feng, A. Gago, L. Timperman, N. Alonso-Vante, *Electrochimica Acta,* 2011, **56**, 1009.

73. P.J. Brown, K.U. Neumann, A. Simon, F. Ueno, K.R.A. Ziebeck, *J Phys-Condens Mat,* 2005, **17**, 1583.

74. M.H. Shao, T. Huang, P. Liu, J. Zhang, K. Sasaki, M.B. Vukmirovic, R.R. Adzic, *Langmuir,* 2006, **22**, 10409.

75. G.A. Tritsaris, J. Rossmeisl, *The Journal of Physical Chemistry C,* 2012, **116**, 11980−11986.

76. I. Chorkendorff, J.W. Niemantsverdriet, Concepts of modern catalysis and kinetics, Wiley-VCH Verlag GmbH & Co KGaA, Weinheim, Germany, 2007.

77. M.H. Seo, S.M. Choi, E.J. Lim, I.H. Kwon, J.K. Seo, S.H. Noh, W.B. Kim, B. Han, *Chemsuschem,* 2014, **7**, 2609.

78. J. Greeley, I. Stephens, A. Bondarenko, T.P. Johansson, H.A. Hansen, T. Jaramillo, J. Rossmeisl, I. Chorkendorff, J.K. Nørskov, *Nature Chemistry,* 2009, **1**, 552.

79. B.J. Kim, D.U. Lee, J. Wu, D. Higgins, A. Yu, Z. Chen, *The Journal of Physical Chemistry C,* 2013, **117**, 26501.

80. D.C. Higgins, J.Y. Choi, J. Wu, A. Lopez, Z. Chen, *Journal of Materials Chemistry,* 2012, **22**, 3727.

81. D. van der Vliet, D.S. Strmcnik, C. Wang, V.R. Stamenkovic, N.M. Markovic, M.T.M. Koper, *Journal of Electroanalytical Chemistry,* 2010, **647**, 29.

82. G. Kresse, J. Furthmüller, *Physical Review B,* 1996, **54**, 11169.

83. P. Hohenberg, W. Kohn, *Physical Review,* 1964, **136**, B864.

84. W. Kohn, L.J. Sham, *Physical Review A,* 1965, **140**, 1133.

85. J.P. Perdew, K. Burke, M. Ernzerhof, *Physical Review Letters,* 1996, **77**, 3865.

86. G. Kresse, J. Furthmuller, *Computational Materials Science,* 1996, **6**, 15.

87. J.P. Perdew, K. Burke, Y. Wang, *Physical Review B,* 1996, **54**, 16533.

88. G. Kresse, D. Joubert, *Physical Review B,* 1999, **59**, 1758

89. P.E. Blöchl, *Physical Review B,* 1994, **50**, 17953.

90. M. Methfessel, A.T. Paxton, *Physical Review B,* 1989, **40**, 3616.
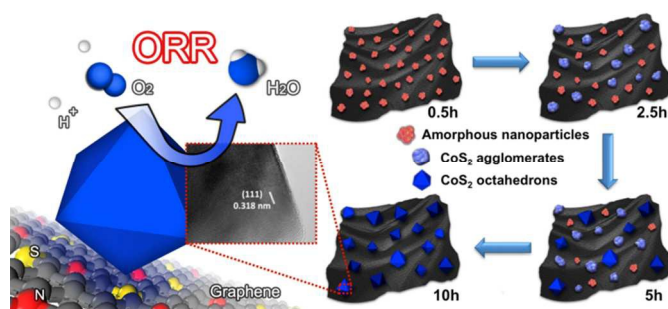
Shape controlled cobalt disulfide octahedron nanoparticles are grown on nitrogen/sulfur-doped carbon nanotube-graphene composites as active non-precious oxygen reduction catalysts.